MSDE

PAPER

View Article Online
View Journal | View Issue

Check for updates

Cite this: *Mol. Syst. Des. Eng.*, 2022, 7, 622

Bayesian optimization for material discovery processes with noise†‡

Sanket Diwale, [a] Maximilian K. Eisner, [b] Corinne Carpenter,[a] Weike Sun,[a] Gregory C. Rutledge*[a] and Richard D. Braatz *[a]

Received 27th October 2021,
Accepted 7th March 2022

DOI: 10.1039/d1me00154j

rsc.li/molecular-engineering

An augmented Bayesian optimization approach is presented for materials discovery with noisy and unreliable measurements. A challenging non-Gaussian, non-sub-Gaussian noise process is used as a case study for the discovery of additives for the promotion of nucleation of polyethylene crystals. NEMD (non-equilibrium molecular dynamics) data are used to validate and characterize the statistical outcomes of the candidate additives and the Bayesian optimization performance. The discovered candidates show nearly optimal performance for silicon for the class of tetrahedrally coordinated crystals and a material similar to graphene but more compliant for the class of hexagonally coordinated crystals. The Bayesian approach using a noise-augmented acquisition function and batched sampling shows a sub-σ level of median accuracy and an improved robustness against noise.

Design, System, Application

The work addresses the data-driven discovery of materials using molecular dynamics and Bayesian optimization. Molecular dynamics provide an inherently stochastic environment for statistical characterization of material properties in simulation. However, the computational cost of such simulations makes it prohibitively expensive to include directly in an iterative learning or optimization scheme. Bayesian optimization addresses this challenge by providing a near-optimal strategy for minimizing the number of iterations required for such a data-driven scheme. We also use a united atomic force field model for material candidates that allows a low-dimensional parametric search space to be used both for molecular simulations and the Bayesian optimization scheme. A polymer melt crystallization process using nucleating agents serves as a case study for the materials discovery problem. A search for agents maximizing the expected nucleation rate is conducted using the Bayesian optimization scheme. A significant challenge in applying Bayesian optimization to noisy processes is that noise can behave as an adversary to the optimization scheme and lead to loss of convergence or significant performance degradation. The work presents a method to augment the Bayesian optimization scheme in the presence of such noise to improve convergence and robustness properties. When applied to the polymer crystallization problem, the algorithm shows a median convergence error of less than one standard deviation of the noise and a worst-case error of less than three standard deviations. A search within a class of tetrahedral nucleating agents suggests a close to optimal performance for silicon. In contrast, a search within a class of hexagonal agents shows that a crystal similar but more compliant than graphene would provide an optimal nucleation rate for polyethylene nucleation.

1 Introduction

Global competitiveness in advanced materials depends on shortening the development cycles for the discovery of new materials. Given the vast monetary and time cost associated with experimental characterization and empirical discovery of new materials, data-driven and simulation-based techniques allow for the rapid discovery and development of promising new material candidates.

Molecular simulations and finite-element methods have long been used for gaining insights into the characteristics and formation mechanics of new material candidates. Embedding these simulations within iterative learning and optimization schemes allows for a computational and data-driven approach to the discovery of new materials. This direct approach, however, faces several challenges.

Firstly, material formation mechanics are inherently stochastic, and thus multiple (stochastic) molecular simulations are required to obtain statistical material characteristics with sufficiently high confidence. Secondly, each molecular simulation incurs a high computational cost and can take anywhere from a few hours to a few days. Embedding such a simulation directly into an iterative learning or optimization scheme can become prohibitively expensive.

Another challenge posed from the numerical optimization perspective is that the number of potential degrees of

[a] *Department of Chemical Engineering, Massachusetts Institute of Technology, Cambridge, MA 02139 USA. E-mail: rutledge@mit.edu, braatz@mit.edu*
[b] *Department of Electrical and Computer Engineering, Technical University of Munich, 80333 Munich, Germany*

† The source code for the work presented in this article may be obtained from https://github.com/sanketdiwale/NoisyBayesianOptimization.

‡ Electronic supplementary information (ESI) available. See DOI: 10.1039/d1me00154j

Open Access Article. Published on 07 March 2022. Downloaded on 6/18/2025 3:41:35 AM.
This article is licensed under a Creative Commons Attribution-NonCommercial 3.0 Unported Licence.

This journal is © The Royal Society of Chemistry and IChemE 2022

Open Access Article. Published on 07 March 2022. Downloaded on 6/18/2025 3:41:35 AM.
This article is licensed under a Creative Commons Attribution-NonCommercial 3.0 Unported Licence.

freedom that define the class of potential molecular formulations is large and include both continuous and discrete variables. These optimizations become especially challenging to solve when the molecular simulations and the resulting objective functions are inherently stochastic. We show in this work that an atomic force field model can be effectively used to parameterize the search space for materials and used with a Bayesian optimization scheme to minimize the number of experiments or simulations required for a materials discovery problem in the presence of noise.

Bayesian optimization addresses the challenges of experimental sample minimization and noise modeling by using a stochastic model to assign information-theoretic value and confidence to the acquired experimental samples. A simultaneous learning and optimization approach is taken to address the exploration-exploitation tradeoff to minimize the number of samples required to discover optimal candidates reliably.

The work in Bayesian optimization may be divided into two parts. The first part considers optimization with noise-free observations of the objective values.[1–6] The second considers optimization in the presence of noisy observations.[7–17]

The primary role of Bayesian uncertainty in such optimization algorithms is to serve as a surrogate for the information-theoretic uncertainty induced by the lack of observed data in the search space. The surrogate allows for the development of decision rules for sampling the objective in an iterative optimization scheme to balance between exploration (to reduce information-theoretic uncertainty) and exploitation (to optimize the intended objective value in the optimization).

By acquiring new samples of data to reduce information-theoretic uncertainty, the optimization scheme progressively learns a better model for the objective function while the exploitation terms in the decision rule bias the exploration towards the regions with good objective values.

The introduction of noise in the observations is known to significantly degrade the performance in Bayesian optimization[12,17] and presents an active area of research.[12–17] The degradation can be attributed to the fact that the Bayesian uncertainty in the presence of noise is used for the dual purpose of representing observation noise as well as information-theoretic uncertainty. The dual use of a single uncertainty model thus creates ambiguity for the decision rules where a high uncertainty value due to noise may obscure the knowledge of high information-theoretic uncertainty, leading to inefficient exploration and the loss of convergence properties.

In recent years, Bayesian optimization has been introduced to many fields, including in robotics,[7–11] software testing,[12] personalized medicine,[18] automated machine learning,[19] reinforcement learning,[20,21] and materials discovery,[22–25] where noisy measurements can significantly degrade the algorithm's performance[12] and thus require further algorithmic and theoretical improvements to support practical applications.

In particular, works for materials discovery using Bayesian optimization[22–25] have focused on the use of Bayesian optimization algorithms designed assuming either noise-free or Gaussian noise assumptions. We present here a practical materials discovery problem example, where such noise assumptions are invalidated and result in significant performance degradation of the previously used Bayesian optimization algorithms. We further show how simple modifications to the decision rules used in the algorithm may improve the robustness of the optimization to the observed noise.

For the materials discovery problem, we consider the process of polymer (polyethylene) nucleation in the presence of a nucleating agent. The process output, given as the observed nucleation time, follows an exponential probability distribution and presents a concrete, challenging, real-world example of a non-Gaussian and non-sub-Gaussian noise process to tackle by Bayesian optimization. Such a noise process falls outside the currently explored theoretical and empirical understanding of Bayesian optimization[15,26–30] that has largely focused on noise-free, Gaussian noise, and sub-Gaussian noise. We highlight some of challenges posed to Bayesian optimization by such noise, and characterize and discuss convergence when dealing with such noise. A noise-augmented approach is shown to perform with a greater degree of robustness and better convergence performance than the traditional Bayesian optimization schemes designed for noise-free or Gaussian noise scenarios.

The type of stochastic models used for Bayesian optimization can be varied and includes probabilistic graphical models,[31] Bayesian neural networks,[32,33] Parzen tree estimators,[34] and Gaussian process models.[7–11] The use of Gaussian process models in Bayesian optimization is by far the most common, owing to the decades of empirical and theoretical exploration of their properties for Bayesian optimization.[15,26–30,35] Gaussian process-based optimization also empirically offers the best performance in low-dimensional parameter spaces due to the higher degrees of freedom involved in training tree- or neural network-based models.[33] For this reason, Gaussian processes are used as the underlying model in this work.

In the following, section 2 describes the polymer nucleation process, and the material discovery problem addressed in this work. Section 3 briefly introduces Bayesian optimization for noisy processes and section 4 discusses theoretical aspects of the algorithm. Section 5 hosts a discussion on the acquisition functions used as a sampling decision rule to choose iterates in Bayesian optimization and introduces the generalized noise-augmented acquisition function used in this work. Section 6 presents numerical results and discussion on the application of the noisy Bayesian optimization algorithm to the materials discovery problem in polymer nucleation. Section 7 highlights some key takeaways from the work and future directions for investigation.

The results show the robustness of the proposed algorithm to a non-Gaussian noise with a median convergence error of less than one standard deviation of the noise and a worst-case error of less than three standard deviations.

Open Access Article. Published on 07 March 2022. Downloaded on 6/18/2025 3:41:35 AM.
This article is licensed under a Creative Commons Attribution-NonCommercial 3.0 Unported Licence.

2 Polymer nucleation: a case study

In polymer crystallization from melts, additives referred to as nucleating agents are used to enhance the crystalline growth rate by lowering the activation energy for nucleation and subsequent crystallization. The nucleating agent's quantity and choice directly control the degree of crystallinity and morphology introduced into the polymer. The agent's effect in crystalline growth is characterized by the nucleation time (also called the induction time τ) that denotes the time instant at which heterogeneous nucleation occurs at the interface between the nucleating agent and the polymer precursor. The induction time at such an interface follows an exponential-like probability distribution[36] of the form

$$p(\tau) \sim \kappa(\tau) \mathrm{e}^{-\int_{t_0}^{\tau} \kappa(t)\mathrm{d}t} \tag{1}$$

where $\kappa(\cdot)$ is a time-varying nucleation rate for the process, and t_0 is the initial time at which the nucleation process begins. The time-varying nucleation rate $\kappa(t)$ captures the effects of a time-varying temperature profile onthe nucleation.[36]

Under the simplifying assumption of time-invariant temperature and nucleation rate κ, (1) simplifies to a standard exponential distribution,

$$p(\tau) \sim \kappa \mathrm{e}^{-\kappa\tau}, \tag{2}$$

with a mean induction time $\tau_{\mathrm{mean}} = 1/\kappa$ and a variance of $1/\kappa^2$.

The nucleation rate for a particular agent depends on its physical and chemical properties and has been studied for *n*-alkanes for tetrahedrally coordinated agents like silicon[37] and for graphene-like materials.[38] A united-atom force field (UAFF) model has been used[37,38] to study the dependence of κ and the induction time on four parametric properties of nucleating agents:

1. σ_{SW}, the atomic diameter of the agent
2. $\varepsilon_{\mathrm{SW}}$, the depth of two-body interaction potential
3. λ_{SW}, relative strength of three body interactions
4. $\varepsilon_{\mathrm{AD}}$, the depth of interaction potential between the agent and crystallizing material.

The first three parameters refer to the Stillinger–Weber (SW) potential[39] used to model the nucleating agent, where σ_{SW} provides a length scale, $\varepsilon_{\mathrm{SW}}$ is a cohesive energy scale, and $\varepsilon_{\mathrm{AD}}$ is an adhesive energy scale between the nucleating agent and the polymer. These properties are readily available for reference materials such as graphene and silicon from the literature, which have been used to normalize parameter values with respect to reference materials.[37,38] We denote normalized values with a * superscript.

By considering the molecular design space to be parameterized by a vector of normalized UAFF parameters,

$$x = \left(\sigma^*_{\mathrm{SW}}, \varepsilon^*_{\mathrm{SW}}, \lambda^*_{\mathrm{SW}}, \varepsilon^*_{\mathrm{AD}}\right),$$

we can denote the nucleation rate per mole of an additive to be denoted as $\kappa(x)$. By systematically varying the values of x over a grid, a response surface $\kappa(x)$ for the dependence of nucleation rate on the above parameters using non-equilibrium molecular dynamic (NEMD) simulations can be obtained.[37,38] These response surfaces provide an estimate of the ground truth for a case study in the application of Bayesian optimization to the noisy, materials (additive) discovery problem in *n*-alkanes using tetrahedral and hexagonal coordinated additives, considered in section 6.

Using NEMD data,[37,38] an estimate for the response surface is constructed using an elastic learning framework[40] to predict the mean induction time $\tau_{\mathrm{mean}}(x)$ as a function of x. This modeling step is not required for the Bayesian optimization scheme. However, this step allows us to define an underlying ground truth to compare convergence results in the Bayesian optimization approach. The model also acts as an inexpensive function evaluation substitute to the significantly more expensive NEMD simulation required to make predictions for an arbitrary candidate x. Using such a substitute allows faster function evaluations and enables running several variations of the Bayesian optimization scheme for a comparative study of their properties in a pragmatic time frame. In a real application, when such a comparative study of variants is not intended, the function evaluations would be directly computed from the output of the expensive NEMD run.

The elastic net provides an exponential indefinite quadratic model of the form (3) for the mean induction time estimate $\hat{\tau}_{\mathrm{mean}}$ as a function of x,

$$\hat{\kappa}(x)^{-1} = \hat{\tau}_{\mathrm{mean}}(x) = \exp\left(x^{\top} Q x + A x + b\right). \tag{3}$$

We consider two separate case studies for the additive discovery problem. The first considers additives in the class of tetrahedral (silicon-like) crystals, and the second for hexagonal (graphene-like) additive crystals with NEMD data from Bourque *et al.*[37,38] Table 1 shows the parameters learned from the two data sets.

Bourque *et al.*[37] restricts the data exploration to only three out of the four parameters, leaving out dependencies on $\varepsilon^*_{\mathrm{SW}}$. To maintain consistency with the available NEMD data, we restrict the Bayesian optimization for the tetrahedral case to

Table 1 Model parameters for the mean induction time models

Case	Q	A	b
Tetrahedral	Q_1	(−382.66 0 0 −10.72)	172.64
Hexagonal	Q_2	(−14.69 0 0 −0.106)	9.457

$$Q_1 = \begin{pmatrix} 227.88 & 0 & -0.28 & -6.53 \\ 0 & 0 & 0 & 0 \\ -0.28 & 0 & 0 & 0.83 \\ -6.53 & 0 & 0.83 & 10.45 \end{pmatrix}$$

$$Q_2 = \begin{pmatrix} 17.27 & 1.56 & -2.27 & -9.34 \\ 1.56 & 0 & 0 & -1.86 \\ -2.27 & 0 & 0 & 2.59 \\ -9.34 & -1.86 & 2.59 & 8.84 \end{pmatrix}$$

This journal is © The Royal Society of Chemistry and IChemE 2022

Open Access Article. Published on 07 March 2022. Downloaded on 6/18/2025 3:41:35 AM.
This article is licensed under a Creative Commons Attribution-NonCommercial 3.0 Unported Licence.

Table 2 Bounds on the search domain

Case	σ^*_{SW}	ϵ^*_{SW}	λ^*_{SW}	ε^*_{AD}
Tetra.	[0.8, 0.95]	—	[0.9, 1.3]	[0.6, 1]
Hexa.	[1.05, 1.33]	[0.28, 0.44]	[0.31, 0.74]	[0.8, 1.2]

the same three parameters. Furthermore, the search space is restricted to the bounded domain of parameters considered in the NEMD data to avoid extrapolation from the data available. The bounded domain intervals are shown in Table 2.

The mean induction time model (3) is then used with (2) to obtain an estimate for the probability distribution for induction time as a function of x. A random sample is drawn from this distribution to provide a noisy realization for the induction time measurement for a candidate x for the Bayesian optimization scheme.

In order to compare the results from Bayesian optimization to the estimate of the underlying ground truth, we run a numerical optimizer on the model (3) to find the minimizer for the mean induction time as

$$\hat{\tau}^{\text{opt}}_{\text{mean}} = \begin{cases} 4.02\ \text{ns} & \text{Tetrahedral case} \\ 7.34\ \text{ns} & \text{Hexagonal case} \end{cases} \tag{4}$$

and

$$\hat{x}_{\text{opt}} = \begin{cases} (0.98, -, 0.9, 0.869) & \text{Tetrahedral case} \\ (1.05, 0.44, 0.31, 1.115) & \text{Hexagonal case} \end{cases} \tag{5}$$

The Bayesian optimization is used in section 6 as an alternative method to find the optimal additive candidate x that minimizes the mean induction time without having the need to construct an *a priori* model of the form (3) or having access to an extensively gridded NEMD data set as obtained from Bourque *et al.*[37,38] With a noisy measurement of induction times, the convergence error of the optimization scheme needs to be evaluated in relation to the variance of the measurement noise. We use the noise standard deviation at the estimated optimal candidate from (4) as a reference to compare the convergence error against. For an exponential distribution, the standard deviation is equal to the mean, and thus we assign the reference standard deviation

$$\sigma_\eta = \hat{\tau}^{\text{opt}}_{\text{mean}} \tag{6}$$

The following sections describe the Bayesian optimization algorithm and its application to the noisy materials-discovery problem and the case studies described above.

3 Noisy Bayesian optimization

This section describes the Bayesian optimization approach to the noisy materials-discovery problem.

Let $\mathscr{X}$ be a set of candidate materials, parameterized by a vector x. Let $f(x)$ be a noisy process with an unknown distribution, which can be sampled *via* experiment for any given x. The Bayesian optimization seeks to find a minimizer to

$$x^{\text{opt}} = \arg\min_{x \in \mathscr{X}} \mathbb{E}[f(x)] \tag{7}$$

Since $f(x)$ is an unknown stochastic process, a stochastic process model $\hat{f}_k(x)$ is learned from a sampled data set of noisy observation tuples $\mathscr{D}_k = \{(x_i, y_i)\colon i = 1, \ldots, k\}$, where y_i is a noisy outcome of the distribution $f(x_i)$.

Several learning methods including probabilistic graphical models,[31] Bayesian neural networks,[32,33] Parzen tree estimators,[34] and Gaussian process models[7–11] have been used to construct a stochastic model $\hat{f}_k(x)$ in Bayesian optimization. Gaussian process models are used in this work, due to the simplicity of the learning method, better empirical performance,[33] and existing theoretical foundations[15,26–30,35] that contextualize the convergence results.

The Gaussian process model[41] provides a Bayesian posterior mean and variance prediction at any query point x, conditioned on the evidence observed from the data set $\mathscr{D}_k$ and a prior mean function $\mu_0(x)$ and prior covariance function $K(x_i, x_j)$. The posterior mean prediction from the model is given by

$$\mu_k(x) = \mu_0(x) + \sum_{i=1}^{k} \alpha_i K(x, x_i) \tag{8}$$

with coefficients α_i given by the members of the $\mathbb{R}^k$ vector,

$$\alpha = [K(X,X) + \sigma_n^2 \mathbb{I}_k]^{-1} (\boldsymbol{y} - \mu_0(X)) \tag{9}$$

with

$$K(X,X) = \begin{pmatrix} K(x_1,x_1) & \ldots & K(x_1,x_k) \\ K(x_2,x_1) & \ldots & K(x_2,x_k) \\ \vdots & \vdots & \vdots \\ K(x_k,x_1) & \ldots & K(x_k,x_k) \end{pmatrix} \tag{10}$$

$$\boldsymbol{y} = \begin{pmatrix} y_1 \\ \vdots \\ y_k \end{pmatrix}, \quad \mu_0(X) = \begin{pmatrix} \mu_0(x_1) \\ \vdots \\ \mu_0(x_k) \end{pmatrix}, \quad K(x,X) = \begin{pmatrix} K(x,x_1) \\ \vdots \\ K(x,x_k) \end{pmatrix}^{\top} \tag{11}$$

and σ_n^2 being the assumed noise variance of an additive Gaussian measurement noise and $\mathbb{I}_k$ being an identity matrix of size k. The posterior covariance is given by

$$\sum_k (x,s) = K(x,s) - K(x,X)\left[K(X,X) + \sigma_n^2 \mathbb{I}_k\right]^{-1} K(X,s) \tag{12}$$

for any $x, s \in \mathscr{X}$.

An additional step of selecting an optimized prior for the Gaussian process, by choosing a particular mean

Open Access Article. Published on 07 March 2022. Downloaded on 6/18/2025 3:41:35 AM.
This article is licensed under a Creative Commons Attribution-NonCommercial 3.0 Unported Licence.

function μ_0 and prior covariance function K within a parameterized space of mean and covariance functions, is often undertaken in Gaussian process learning, given the data set $\mathscr{D}_k$. The parameters used to parameterize this space of function choices for μ_0, K are called hyperparameters and are learned using a Bayesian or maximum likelihood approach.[41]

The optimization of hyperparameters based on $\mathscr{D}_k$ is, however, known to cause over-fitting problems and loss of convergence guarantees in Bayesian optimization.[26,30] As a result, most Bayesian optimization schemes with convergence guarantees rely on either using fixed hyperparameters[15,26] or a scheduling or error-based adaptive approach to hyperparameter selection.[27–29]

The second element of Bayesian optimization is a decision rule, selecting the next batch of iterates to be sampled *via* experiment. Given the stochastic model $\hat{f}_k$, an acquisition function $A(x|\hat{f}_k)$ assigns a merit value to each potential sampling location x in the search space. This value is meant to trade off the value of exploring the search space against the value of exploiting current model knowledge based on $\mathscr{D}_k$. Exploration allows finding new potential optimal candidates that the model $\hat{f}_k$ cannot yet predict due to the lack of relevant data in $\mathscr{D}_k$ while exploiting the existing model $\hat{f}_k$ allows choosing sample points that are most likely to provide optimal candidates within the limitations of model. Some examples of such acquisition functions are shown in Table 3 and discussed in detail in section 5.

Let q be the batch size of candidates to be acquired at each iteration of the optimizer. The next batch of candidate samples for experiments are then selected as maximizers of the acquisition function A,

$$x_{k+1}, \ldots, x_{k+q} = \underset{s_{k+i} \in \mathscr{X}, i=1,\ldots,q}{\arg\max}\ A\left(s_{k+1}, \ldots, s_{k+q} | \hat{f}_k\right). \tag{13}$$

The sampled experimental data $\{(y_{k+i}, x_{k+i})\colon i = 1,\ldots,q\}$ acquired from the proposed candidates are appended to the data set to obtain $\mathscr{D}_{k+q} = \mathscr{D}_k \cup \{(y_{k+i}, x_{k+i})\colon i = 1,\ldots,q\}$ and the learned stochastic model is updated with the new data set to provide a model $\hat{f}_{k+q}$. Estimates for the optimal value $\hat{f}^{\text{opt}}_{k+q}$ and optimal candidate x^{opt}_{k+q} are then obtained from the updated model $\hat{f}_{k+q}$ within its trust region, typically chosen as the set of points where sufficient sampling has occurred. We consider the observed set of points $\{x_1,\ldots,x_{k+q}\}$ as the trust region for the model, and estimate optimal candidate as the point with the minimum expected value forthe stochastic model $\hat{f}_{k+q}$,

$$x^{\text{opt}}_{k+q} = \underset{x \in \{x_1,\ldots,x_{k+q}\}}{\arg\min}\ \mathbb{E}\left[\hat{f}_{k+q}(x)\right] \tag{14}$$
$$\hat{f}^{\text{opt}}_{k+q} = \mathbb{E}\left[\hat{f}_{k+q}\left(x^{\text{opt}}_{k+q}\right)\right]$$

The updated model $\hat{f}_{k+q}$ is then used to compute the next batch of candidate samples using the acquisition function as done in (13), and the iterations are repeated until convergence is detected.

Fig. 1 shows a flowchart for the Bayesian optimization algorithm described above with $q = 1$ chosen for simplicity. A termination condition (aka convergence) is said to be reached if a predefined maximum number of iterations is reached or if the maximum value for the acquisition function falls below a threshold value and no change in the optimal candidate value is observed over several iterations. The Bayesian optimization is then said to be complete, and the last updated optimal candidate x^{opt}_{k+q} is declared as the optimal candidate.

A few limitations to the Bayesian optimization approach may be kept in mind when designing such an algorithm. The first relates to the dimension of the search space. It is known from theory[26] that near-optimal bounds for the convergence errors are on the order of $\mathscr{O}\left(\frac{1}{k^{1/d}}\right)$ in a d-dimensional search space after k iterations of the algorithm. Thus, as the dimension of the search space d increases, the log of the error by a multiplicative factor d. This can make the application of the Bayesian optimization approach to large dimensional search spaces difficult in practice.

The second limitation relates to the increasing computational complexity $\mathscr{O}(n^3)$ of kernel-based learning methods such as Gaussian process models with increasing size n of the training set. This limitation may be overcome by usinga parameterized model, such as a generalized linear model or a neural network with a fixed set of basic functions or feature mappings. The use of a generalized linear model may, however, limit the expressiveness of the model, and the use of a neural network may not be amenable to practical training with the small sizes of the training sets expected from a Bayesian optimization algorithm. A practical approach

Table 3 Example acquisition functions

Acquisition function	Form
Expected improvement (EI)	$\mathbb{E}[\max(\hat{f}^{\text{opt}}_k - \hat{f}_k(x), 0)]$
Lower confidence bound (LCB)	$\mathbb{E}\left[\hat{f}_k(x)\right] - \beta_k \sqrt{\text{Var}\left[\hat{f}_k(x)\right]}$

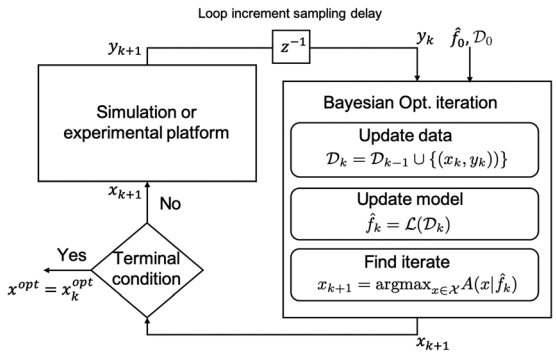

Fig. 1 Bayesian optimization flowchart. ($\mathscr{L}(\mathscr{D}_k)$ is used to denote the learning method of choice being applied to a data set $\mathscr{D}_k$).

This journal is © The Royal Society of Chemistry and IChemE 2022

Open Access Article. Published on 07 March 2022. Downloaded on 6/18/2025 3:41:35 AM.
This article is licensed under a Creative Commons Attribution-NonCommercial 3.0 Unported Licence.

may be to use a randomized feature map that approximates a kernel, as proposed by Ueno *et al.*[22]

The third limitation is the lack of *a priori* bounds on the number of iterations required to find a good quality solution. The algorithm typically provides an asymptotic convergence bound, but the exact number of required iterations remains subject to trial and error and empirical observation. Section 4.1 presents a detailed discussion on characterizing the convergence error and provides a sketch for proof towards establishing a convergence bound in the presence of noise. An important insight that may be gained from the discussion is that obtaining a low convergence error with high probability requires repeated sampling at the observed candidates in the optimization algorithm. An acquisition function that promotes such repeated sampling is thus important for the reliable operation of the algorithm in the presence of noise. Section 4.2 discusses the empirical characterization of convergence in such noisy scenarios.

4 Convergence analysis

4.1 Theoretical analysis

Given a declaration of an optimal candidate x_k^{opt} and $\hat{f}_k^{\text{opt}}$ after acquiring k data samples as in (14), the ability of the algorithm to converge to the true (but unknown) optimal values of $x_{\text{true}}^{\text{opt}}$ and $f_{\text{true}}^{\text{opt}}$ can be measured in terms of the convergence errors,

$$\delta f_{\text{opt}}^k = \left|\hat{f}_k^{\text{opt}} - f_{\text{true}}^{\text{opt}}\right| \;\&\; \delta x_{\text{opt}}^k = \left\|x_k^{\text{opt}} - x_{\text{true}}^{\text{opt}}\right\|. \tag{15}$$

The convergence error δf_{opt}^k is called the *instantaneous regret* after acquiring k samples. Similarly, the cumulative sum $\delta f_{\text{opt}}^{1:k} = \sum_{i=1}^{k} \delta f_{\text{opt}}^i$ is called the *cumulative regret*. An algorithm is said to have the desirable asymptotic property of *no-regret* if the limit $\lim_{k\to\infty} \delta f_{\text{opt}}^{1:k}/k = 0$.

In most cases, the true optimal values are unknown. Thus the convergence errors in (15) cannot be directly measured. Instead, only a probabilistic bound on the expectation of these regrets can be made, based on the model assumptions and number of observed samples in the data set.

One such bound,[26] for the noise-free case of Bayesian optimization in a d-dimensional search space is

$$\mathbb{E}\left[\delta f_{\text{opt}}^k\right] \sim \mathcal{O}\left(\frac{1}{k^{1/d}}\right) \tag{16}$$

where the big-$\mathcal{O}$ notation is used to describe the asymptotic behavior of the expected instantaneous regret. Eqn (16) shows that, if the underlying true function is at least twice differentiable and continuous (C^2 function), with noise-free measurements, the expected regret asymptotically converges towards zero faster than the function $k^{-1/\text{d}}$.

With noisy measurements, an additional challenge is encountered due to the errors incurred in learning the error-free true mean values. In the noise-free case, kernel-based learning methods like the Gaussian process learning, provide an error-free prediction of the mean value at the observed candidate points $\{x_1,\ldots,x_k\}$. However, for the noisy case, the measurements y_i are polluted with noise and the prediction error

$$\eta_f(x) = \mathbb{E}[\hat{f}_k(x)] - \mathbb{E}[f(x)] \tag{17}$$

is non-zero at the observed locations in $\mathscr{D}_k$. An error in the mean value prediction directly affects the value computed by the acquisition function and causes an error in the optimal estimates obtained from (14). Thus noise in the measurement can act as an adversary in the Bayesian optimization scheme and lead to a loss of convergence properties.

The convergence of a Bayesian scheme in the presence of noise thus relies on drawing multiple samples around the already sampled locations in $\mathscr{D}_k$ to reduce the prediction error η_f. A significant degradation in the convergence properties for Bayesian optimization can be observed empirically[13,42,43] with noisy measurements, when using the standard expected improvement (EI) or lower confidence bound (LCB) acquisition functions (Table 3). While convergence to the optimum can still be guaranteed with Gaussian noise,[15] the convergence is shown empirically to be much slower with the standard EI or LCB acquisition functions.[42] The noise-augmented EI and knowledge-gradient (KG) acquisition functions are known to have much better empirical convergence rates with noisy measurements.[12,43]

Furthermore, the convergence of Bayesian optimization schemes in the presence of a non-(sub) Gaussian noise distribution such as considered in section 2 is not yet established theoretically. The additional challenge posed by such distributions when using a Gaussian process model is the structural mismatch in the learned stochastic process (Gaussian) and the real underlying stochastic process (f). With finite repeated sampling at a given location x, the prediction error $\eta_f(x)$ may still remain large, thus leading to slower convergence or adversarial effects of the noise in Bayesian optimization. These difficulties are shown empirically in section 6. However, Section 6 shows empirically that a combination of batched sampling and a generalized noise-augmented EI acquisition function can still be used to provide an improved convergence and robustness in Bayesian optimization with such structural mismatches.

A non-zero prediction error $\eta_f(x)$ implies a non-zero expected error in the optimal candidate estimates,

$$\delta x_{\text{opt}}^k = \left\| \arg\min_{x\in\{x_1,\ldots,x_k\}} \mathbb{E}\left[\hat{f}_k(x)\right] - x_{\text{true}}^{\text{opt}} \right\|. \tag{18}$$

Recalling the definitions (17) and $x_{\text{true}}^{\text{opt}} = \arg\min_{x\in\mathscr{X}} \mathbb{E}[f(x)]$, a rearrangement of terms is be used to rewrite δx_{opt}^k as

Open Access Article. Published on 07 March 2022. Downloaded on 6/18/2025 3:41:35 AM.
This article is licensed under a Creative Commons Attribution-NonCommercial 3.0 Unported Licence.

$$\delta x^k_{\text{opt}} = \left\| \arg\min_{x\in\{x_1,\ldots,x_k\}} \eta_f(x) + \arg\min_{x\in\{x_1,\ldots,x_k\}} \mathbb{E}[f(x)] - \arg\min_{x\in\mathscr{X}} \mathbb{E}[f(x)] \right\|$$
$$\leq \left\| \arg\min_{x\in\{x_1,\ldots,x_k\}} \eta_f(x) \right\| + \left\| \arg\min_{x\in\{x_1,\ldots,x_k\}} \mathbb{E}[f(x)] - \arg\min_{x\in\mathscr{X}} \mathbb{E}[f(x)] \right\| \quad (19)$$

This expression splits the error in optimal candidate estimation into two parts shown on the right-hand side of the inequality. The first part $\left(\left\|\arg\min_{x\in\{x_1,\ldots,x_k\}} \eta_f(x)\right\|\right)$ relates to the prediction error (17) in the model, while the second part relates to the exploratory error for the optimization arising from the limited trust region of the model ($\{x_1,\ldots,x_k\} \subset \mathscr{X}$).

If the expectation of the true stochastic process ($[\mathbb{E}f(x)]$) is assumed to be Lipschitz continous with a Lipschitz bound L, then an error in optimal candidate estimation δx^k_{opt} leads to a worst-case estimation error in the optimal value $\delta f^k_{\text{opt}} \leq L\delta x^k_{\text{opt}}$. The effect of prediction and exploratory errors on δx^k_{opt} is then proportional to their effect on δx^k_{opt}.

For the noise-free case, Gaussian process learning can provide a zero prediction error $\left(\left\|\arg\min_{x\in\{x_1,\ldots,x_k\}} \eta_f(x)\right\| = 0\right)$ at the observed points, while the exploratory error follows an asymptotic convergence as shown in (16).

For the noisy case, we must rely on repeated sampling at the locations in $\{x_1,\ldots,x_k\}$ to drive the prediction error $\left\|\arg\min_{x\in\{x_1,\ldots,x_k\}} \eta_f(x)\right\|$ towards zero. The need for repeat sampling thus slows down the convergence rate for the exploratory error and may lead to a non-zero prediction error at termination due to the finite nature of repeated sampling in a practical algorithmic setting.

With repeated sampling at a given location, assuming negligible covariance to other locations, the worst-case convergence rate for the prediction error can be expected to follow a normal distribution $\eta_f(x) \sim \mathcal{N}(0, \sigma^2_\eta(x)/n(x))$ using the central limit theorem, where $\sigma^2_\eta(x)$ is the noise variance at x and $n(x)$ is the number of samples drawn at location x.

A Bayesian optimization scheme with the underlying assumptions and conditions of (16), taking N repeated samples for every location sampled in $\mathscr{D}_k$, follows an exploratory error convergence rate of $\mathcal{O}(1/(N^{-1}k^{1/d}))$. The overall error in δx^k_{opt} can then be analyzed as an asymptotic convergence resulting from the sum of the two converging error components.

Repeated sampling at the optimal location $x^{\text{opt}}_{\text{true}}$ will lead to a prediction error $\eta_f(x^{\text{opt}}_{\text{true}}) \sim \mathcal{N}(0, \sigma^2_n(x^{\text{opt}}_{\text{true}})/N)$. The convergence error in the estimated optimal value $\delta f^k_{\text{opt}} \sim |\eta_f(x^{\text{opt}}_{\text{true}})|$ then has the expected value of the half-normal distribution, $\mathbb{E}\left[\delta f^k_{\text{opt}}\right] \sim \sqrt{2/\pi}\sigma_n(x^{\text{opt}}_{\text{true}})/\sqrt{N}$ and variance $\text{Var}[\delta f^k_{\text{opt}}] \sim (1 - 2/\pi)\sigma^2_n(x^{\text{opt}}_{\text{true}})/N$.

We can thus expect to see a non-zero convergence error on average in noisy Bayesian optimization with magnitude on the order of $\sigma_\eta/\sqrt{N}$, ($\sigma_\eta = \sigma_n(x^{\text{opt}}_{\text{true}})$). We observe this phenomena in section 6 with σ_η for the case studies defined in section 2. We characterize the performance of achieving an expected error of less than one standard deviation of the noise (σ_η) with the name, sub-σ convergence or accuracy.

The above discussion is an outline of the arguments behind the convergence expected from a Bayesian optimization scheme in the presence of noise. A further formalization of the proof must take into account the effects of covariance between the data samples that are left out of the above discussion for simplicity.

Section 5 introduces some of the acquisition functions used in Bayesian optimization and introduces the generalized form of the noise-augmented Expected Improvement acquisition used in this work that promotes a data-dependent strategy for repeated sampling to selectively drive the prediction error $\eta_f(x)$ down for the optimal candidates.

4.2 Empirical analysis

While the theoretical analysis of section 4.1 provides insights into the convergence rate statistics up to a proportionality factor, in practice, the factor is unknown and problem-dependent. Thus the theoretical bounds may not be amenable to characterize the number of samples required to guarantee convergence. Instead, one may empirically observe the rate of change of the optimal estimate with the iterations of the algorithm.

Typically, a budget of N samples is decided beforehand for the optimization, and the optimization is terminated after the acquisition of N samples. The last N_{test} samples of the N samples may be used as a test set to characterize the convergence.

The rate of change in the observed function value ($\hat{x}^{\text{opt}}_k$) is observed using the variance of the observed values over the test set. If the variance is smaller than a small threshold ε, the optimization is likely converged, if not, the budget for the samples N may need to be increased further.

The convergence characteristics of the Bayesian optimization scheme vary from one run of the algorithm to another due to the randomized nature of acquired samples. The statistical characterization of the algorithm performance on a problem thus requires multiple independent runs. The algorithm's reliability is then evaluated by observing the variance in convergence characteristics across the multiple runs. Eqn (20) below proposes a quality metric (Q) for the algorithm across L independent multiple runs.

$$Q(f) = \max_{k\in N_{\text{test}}} \text{Var}\left[f\left(\hat{x}^{\text{opt}}_{k,1}\right), f\left(\hat{x}^{\text{opt}}_{k,2}\right), \ldots, f\left(\hat{x}^{\text{opt}}_{k,L}\right)\right] \quad (20)$$

where $\hat{x}^{\text{opt}}_{k,i}$ denotes the estimated optimal candidate at the kth iteration from the ith independent run of the algorithm. The variance $\text{Var}[f(\hat{x}^{\text{opt}}_{k,1}), f(\hat{x}^{\text{opt}}_{k,2}),\ldots,f(\hat{x}^{\text{opt}}_{k,L})]$ is taken across the L observed function values in the independent runs, at each iteration k in the test set. The quality metric Q then takes the worst case variance observed in the test set as a measure for the reliability or quality of the algorithm's design choices. A small value for Q, implies a small worst

This journal is © The Royal Society of Chemistry and IChemE 2022

Open Access Article. Published on 07 March 2022. Downloaded on 6/18/2025 3:41:35 AM.
This article is licensed under a Creative Commons Attribution-NonCommercial 3.0 Unported Licence.

case variance and thus a higher reliability or quality for the algorithm.

The worst-case variance observed in the test set indicates the worst-case convergence result that may be expected if any one of the independent runs was realized during the application of the algorithm to a problem and if the algorithm was randomly terminated at any iteration in the test set. Since the exact number of iterations required for reliable convergence is often unknown, such a worst-case characterization for the convergence result provides an important insight into the algorithm's reliability.

The function f in eqn (20) may be replaced by other functions such as the expected value of f or the regret function if the underlying ground truth for a problem is known, to provide additional insights into the convergence characteristics.

5 Acquisition functions

An acquisition function $A(x|\hat{f}_k)$ evaluates the merit of choosing a candidate point x for sampling to drive down the prediction and exploratory errors (introduced in section 4) in a Bayesian optimization scheme. The next point to sample within a Bayesian optimization algorithm is then found as the point that maximizes the acquisition function, *i.e.*,

$$x_{k+1} = \arg\max_{x\in\mathscr{X}} A\left(x|\hat{f}_k\right) \tag{21}$$

The simplest form of acquisition function is provided by the probability of improvement (POI),

$$A_{\mathrm{POI}}(x|\hat{f}_k) = \mathbb{P}(\hat{f}_k(x) \le \hat{f}_k^{\mathrm{opt}}) \tag{22}$$

where $\hat{f}_{k-1}^{\mathrm{opt}}$ is the current best estimate for the optimal value. This kind of acquisition function represents the greedy approach to candidate sampling, where the sample showing the best probability of improvement according to the current model is chosen as the next candidate to acquire. While simple in formulation, the approach can suffer from non-convergence to the global (or even local) optimum of f, that is, the sampling scheme may fail to acquire samples improving model information and may converge to the optimum of an incorrect model $\hat{f}_N$. In this scenario, the exploratory error component of the expected convergence error in (19) is left undiminished, leading to a large error.

This shortcoming of the greedy approach is overcome by the Expected Improvement (EI) metric[1] which explicitly accounts for the information gained by sampling at a point x in addition to the improvement in the objective value. The metric is computed as the expectation of the objective value at x exceeding the previous best f_k^{opt},

$$A_{\mathrm{EI}}(x|\hat{f}_k) = \mathbb{E}[\max(\hat{f}_k^{\mathrm{opt}} - \hat{f}_k(x), 0)]. \tag{23}$$

A nearly optimal rate of convergence to the global optimum is achieved by the EI acquisition function[26] under assumptions of noise-free, smooth, differentiable underlying functions $f, \hat{f}_k$ in $C^{2\nu}$ for any $\nu > 0$.§ For a Gaussian process model $\hat{f}_k(x) \sim \mathcal{N}(\mu_k(x), \sigma_k^2(x))$, the expected improvement can be written explicitly in terms of the predicted mean and variance as

$$\begin{aligned} A_{\mathrm{EI}}(x|\mu_k, \sigma_k) = {} & \left[\hat{f}_k^{\mathrm{opt}} - \mu_k(x)\right] \Phi\left(\frac{\hat{f}_k^{\mathrm{opt}} - \mu_k(x)}{\sigma_k(x)}\right) \\ & + \sigma_k(x)\, \phi\left(\frac{\hat{f}_k^{\mathrm{opt}} - \mu_k(x)}{\sigma_k(x)}\right) \end{aligned} \tag{24}$$

where Φ and ϕ are the cumulative and probability density functions for the standard normal distribution, respectively.

The expected improvement metric can be seen as a weighted sum between the improvement in mean ($\mu_k(x) - \hat{f}_k^{\mathrm{opt}}$) and standard deviation $\sigma_k(x)$ weighted by cumulative probability and probability density functions respectively. The weighted standard deviation term in (24) provides the acquisition function some value in sampling points where $\sigma_k(x)$ is large, thus promoting exploration in the parameter space, even when the corresponding point x has a low probability of improvement according to A_{POI}. This exploratory quality is known to guarantee asymptotic convergence to the global optimum.[26]

A generalized version of the expected improvement[3] is computed by using an integer power g of max $(\hat{f}_k^{\mathrm{opt}} - \hat{f}_k(x), 0)$ to compute the generalized expected improvement (gEI) as

$$A_{\mathrm{gEI}}(x|\hat{f}_k) = \mathbb{E}[[\max(\hat{f}_k^{\mathrm{opt}} - \hat{f}_k(x), 0)]^g] \tag{25}$$

Using a larger power g promotes the standard deviation terms in the expected improvement and thus promotes more aggressive exploration in the parameter space. For $g = 0$, A_{gEI} is equal to A_{POI} and $g = 1$ gives A_{EI}. For a general integer g and a Gaussian process model $\hat{f}_k(x) \sim \mathcal{N}(\mu_k(x), \sigma_k^2(x))$, the generalized expected improvement can be computed recursively using

$$A_{\mathrm{gEI}}\left(x|\mu_k, \sigma_k, \mathscr{D}_k\right) = [\sigma_k(x)]^g \sum_{i=0}^{g} (-1)^i \binom{g}{i} \left(\frac{\hat{f}_k^{\mathrm{opt}} - \mu_k(x)}{\sigma_k(x)}\right)^{g-i} T_i \tag{26}$$

with

$$T_0 = \Phi\left(\frac{\hat{f}_k^{\mathrm{opt}} - \mu_k(x)}{\sigma_k(x)}\right) \text{ and } T_1 = -\phi\left(\frac{\hat{f}_k^{\mathrm{opt}} - \mu_k(x)}{\sigma_k(x)}\right)$$

Another form of acquisition function used to tradeoff between exploration and exploitation is given by the lower confidence bound (LCB),[44]

§ $C^{2\nu}$ denotes the space of real-valued functions that are differentiable 2ν times with continuous derivatives.

Open Access Article. Published on 07 March 2022. Downloaded on 6/18/2025 3:41:35 AM.
This article is licensed under a Creative Commons Attribution-NonCommercial 3.0 Unported Licence.

$$A_{\mathrm{LCB}}(x|\mu_k, \sigma_k) = \mu_k(x) - \beta_k\sigma_k(x), \tag{27}$$

with some parameter sequence $\beta_k > 0$. The LCB assigns each point an optimistic additive term as a constant β_k multiple of the standard deviation at that point. This additive term promotes exploration; the larger the β_k, the more aggressive the exploration. The factor β_k may be fixed to a constant β throughout the iterations. However, certain k-dependent β_k sequences are shown to provide theoretical convergence bounds for the optimization algorithm.[15,44] The proposed β_k sequences gradually increase the aggressiveness of the search as k increases, with growth on the order of $\mathcal{O}(\sqrt{\ln k})$. The LCB acquisition function is motivated by its simplicity for use with Gaussian process models and is shown to perform at par with the expected improvement function.[15,44]

Unlike the above acquisition functions that are designed with asymptotic convergence in mind,[45] introduced the knowledge gradient (KG) acquisition function to find a nearly optimal solution with only a limited budget for iterations. For $A_{\mathrm{KG}}(x|\hat{f}_k)$, each new sample point is determined by assuming that it is the last available function evaluation in the budget of the Bayesian optimization algorithm. Thus the metric is designed to find the point that maximizes the best possible improvement expected by sampling a point x,

$$A_{\mathrm{KG}}\left(x|\hat{f}_k\right) = \min_{x'\in\mathscr{X}}\mu_k(x') - \mathbb{E}\left(\min_{x'\in\mathscr{X}}\mu_{k+1}(x'|x_{k+1} = x)\right). \tag{28}$$

This equation relies on the closed-form update of the posterior mean of the Gaussian process model when a new point $(x_{k+1} = x, y)$ is added to the training set for the model. The probability of seeing a measurement y for the sample point $x_{k+1} = x$ is taken to be specified by the model $\hat{f}_k \sim \mathcal{N}(\mu_k(x), \sigma_k^2(x))$ and the expectation is taken over this distribution. The closed-form expression of the updated mean after adding a point $(x_{k+1} = x, y)$ for a Gaussianprocess model can be written as

$$\mu_{k+1}(x'|x_{k+1} = x) = \mu_k(x') + \sum(x', x)(\sum(x, x) + \lambda I)^{-1}(y - \mu_k(x)) \tag{29}$$

for a kernel matrix function $\sum(x', x)$ specified for the Gaussian process model and a noise covariance λ assumed for the measurement noise in y.[45] This closed-form expression can be maximized as a function of x' for any given x, y and the expectation over of this maximum as a function of y is taken over the distribution $y \sim \mathcal{N}(\mu_k(x), \sigma_k^2(x))$. This overall computation for the KG acquisition function can become computationally intractable and often requires some form of randomized Monte-Carlo approximation. The next point to acquire x_{k+1} is then obtained by maximizing A_{KG} over the candidate sample space, each evaluation of which requires a Monte-Carlo approximation. This step makes the use of the KG acquisition function computationally expensive.

In addition to the above, the acquisition functions can also be supplemented with additional trust-region constraints or penalties to enforce requirements such as model safety, safe exploration, or dynamical constraints[7–11] leading to further variants.

The above acquisition functions focus on driving down the exploratory error in (19) and make no explicit attempts at repeated sampling to drive down prediction errors for noisy scenarios, which leads to poor convergence performance when working with noisy measurements.[12]

Latham *et al.*[12] use a Monte-Carlo scheme of constructing multiple models $\hat{f}_k^{(i)}$ from artificially generated noise realizations from the model $\hat{f}_k$. An averaged expected improvement using each model is then computed as

$$A_{\mathrm{MC}}\left(x|\hat{f}_k\right) = \frac{1}{N}\sum_{i=1}^{N} A_{\mathrm{EI}}\left(x|\hat{f}_k^{(i)}\right). \tag{30}$$

The averaged EI value over several noise realizations tries to capture a more realistic value of the expected improvement, not adversarially affected by any single noise realization. This approach promotes the repeated sampling required to improve the predictive error component of the convergence error and thus shows improved empirical performance.[12]

Huang *et al.*[13] introduced the augmented EI acquisition function

$$A_{\mathrm{aEI}}(x) = A_{\mathrm{EI}}\left(x|\hat{f}_k\right)\left(1 - \frac{\varepsilon}{\sigma_k^2(x) + \varepsilon}\right) \tag{31}$$

where $\varepsilon > 0$ is a tolerance hyperparameter and $\sigma_k^2(x)$ is the variance prediction at x from the model $\hat{f}_k$. The multiplicative augmentation to the expected improvement metric in (31) increases the value assigned to points with high variance prediction $\sigma_k^2(x)$ given by the model. The variance prediction $\sigma_k^2(x)$ asymptotically decreases to the noise variance σ_n^2 hyperparameter value for a Gaussian process model with repeated sampling at x. The augmentation thus captures the amount of resampling at x as an internal state of the acquisition function and provides a way to enforce resampling at points with high noise variance in order to reduce predictive errors.

We consider a generalized form of the augmentation in (31) and construct the generalized noise-augmented expected improvement as

$$A_{\mathrm{aEI}} = A_{\mathrm{EI}}\left(x|\hat{f}_k\right)\left(1 - \frac{\varepsilon}{\sigma_k^2(x) + \varepsilon}\right)^p \tag{32}$$

for any integer $p \geq 0$. The value $p = 0$ makes $A_{\mathrm{aEI}} = A_{\mathrm{EI}}$ and, with higher values of p, the augmentation sees a sharper increase towards 1 as the variance $\sigma_k^2(x)$ increases. An improved convergence error and robustness is observed as p is increased from 0 to 2 in section 6.

The maximization of the expected improvement or augmented expected improvement can be performed using a gradient-based numerical optimizer. The gradient computations, although tractable, increase the computational

This journal is © The Royal Society of Chemistry and IChemE 2022

Open Access Article. Published on 07 March 2022. Downloaded on 6/18/2025 3:41:35 AM.
This article is licensed under a Creative Commons Attribution-NonCommercial 3.0 Unported Licence.

effort required. Also, gradient-based methods tend to get stuck in local optima for the acquisition functions, which tend to be multi-modal, *i.e.*, have multiple local and global maxima. The multiple maxima can lead to the Bayesian optimizer getting stuck in a local exploration region. These limitations can be overcome by treating the acquisition function as a target probability distribution for a Markov Chain Monte Carlo (MCMC) sampler.[46] The MCMC sampler can draw q samples for any integer q from a probability distribution proportional to the target acquisition function. Since $A_{\mathrm{aEI}}(x|\hat{f}_k) \geq 0$ for all x, the acquisition function can be directly set as the target distribution and used to draw q samples from a probability distribution proportional to $A_{\mathrm{aEI}}(x|\hat{f}_k)$ with an MCMC sampler. This approach allows a simple and direct extension of the acquisition function to a batched sampling approach. Batched sampling further promotes repeated sampling and helps reduce prediction errors. Section 6 compares the convergence performances for different batch sizes q.

6 Results

The Bayesian optimization algorithm from section 3 is run on the case studies for polymer nucleation described in section 2. The algorithm is run with a fixed budget of two thousand samples and compared across ten independent runs for statistical characterization of the convergence properties. A comparison is made using different choices for the generalized noise-augmented acquisition function (32), sample batch sizes q and with a prior-art algorithm for Bayesian optimization in material discovery from Ueno *et al.*[22]

The performance of the algorithm is compared using metrics for optimality, convergence rate, and the quality metric Q to account for the reliability or expected variability in results across different runs. The optimality of the result is characterized by observing a normalized regret

$$\Delta f_{\mathrm{opt}}/\sigma_\eta = \frac{\left|\mathbb{E}[f](\hat{x}_k^{\mathrm{opt}}) - f_{\mathrm{true}}^{\mathrm{opt}}\right|}{\sigma_\eta} \tag{33}$$

where the ground truth estimates for the case studies from Section 2 provide the required quantities $\mathbb{E}[f](x)$ as $\hat{\tau}_{\mathrm{mean}}(x)$ from (3), $f_{\mathrm{true}}^{\mathrm{opt}}$ as $\hat{\tau}_{\mathrm{mean}}^{\mathrm{opt}}$ from (4) and σ_η as the reference standard deviation from (6). The gridded NEMD data[37,38] provides an estimate for the ground truth for the two case studies and are used to characterize the convergence of the algorithm using (33). The algorithm, however, is not provided any knowledge of this underlying ground truth.

6.1 Bayesian optimization with noise-augmented acquisition applied to the polymer nucleation case studies

Fig. 2 and 3 show the typical convergence performance for the algorithm over the two case studies of polymer nucleation presented in section 2, using a batch size of 10 ($q = 10$) and a noise-augmented expected improvement acquisition function ($p = 2$).

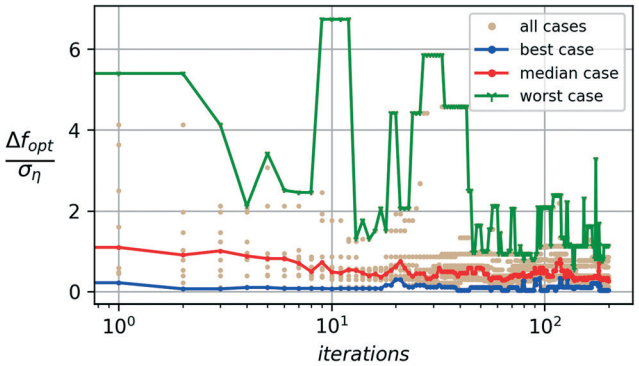

Fig. 2 Tetrahedral additives: A distribution of convergence performance for augmented Expected Improvement $A_{\mathrm{augEI}}(x)$-based Bayesian optimization. A batch of 10 independent runs of 200 iterations is shown with best-case, worst-case, and median performances.

The noisy nature of the process implies that the Bayesian optimization cannot guarantee a zero convergence error to the noise-free optimal solution. Instead, the convergence error is compared to the standard deviation of the noise using the normalization.

The presence of noise also implies that different independent runs of the optimization see different realizations of the noise and thus lead to different convergence paths towards the optima. The algorithm's performance is thus characterized in terms of the observed distribution. Fig. 2 and 3 show the convergence error distribution over a group of 10 independent runs each for the tetrahedral and hexagonal additive groups respectively. The median case shows the median error across runs. The best- and worst-case performances show the minimum and maximum convergence error seen across the different runs at each iteration.

In both cases, we observe a median error of less than one standard deviation of the process noise and a worst-case

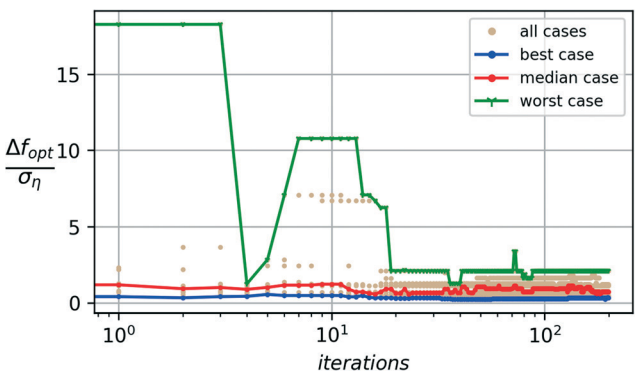

Fig. 3 Hexagonal additives: a distribution of convergence performance for augmented expected improvement $A_{\mathrm{augEI}}(x)$-based Bayesian optimization. A batch of 10 independent runs of 200 iterations is shown with best-case, worst-case, and median performances.

Open Access Article. Published on 07 March 2022. Downloaded on 6/18/2025 3:41:35 AM.
This article is licensed under a Creative Commons Attribution-NonCommercial 3.0 Unported Licence.

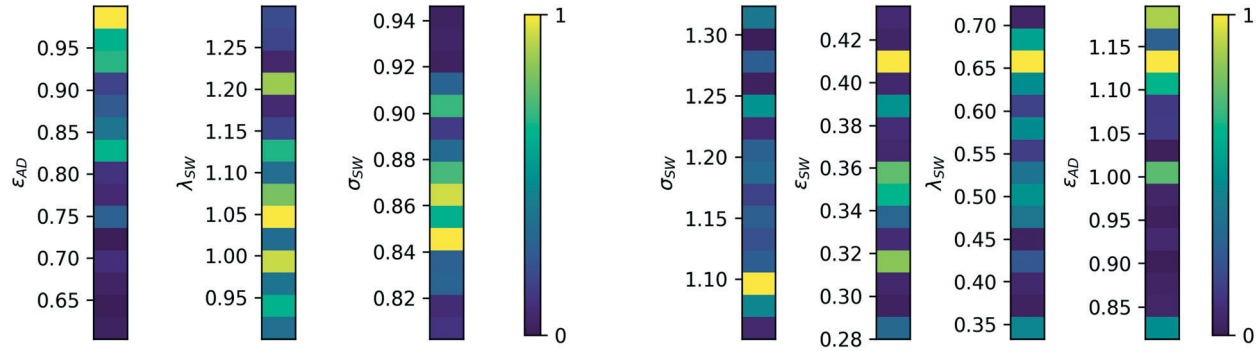

(a) Tetrahedral case study: Parameters normalized with respect to silicon

(b) Hexagonal case study: Parameters normalized with respect to graphene

Fig. 4 Distribution of estimated optimal candidates after 200 iterations of Bayesian optimization.

deviation of less than three standard deviations. A sub-σ level of convergence for the algorithm shows the algorithm's effectiveness in estimating the optimal values with an accuracy level better than the underlying process noise. We observe that, on average, the algorithm performs at this sub-σ level. Even in the worst case, the error in the optimal estimate remains with a $3-\sigma$ level of the noise. The corresponding estimates of the optimal candidate SW-parameters discovered are shown in Fig. 4a and b.

Fig. 4a and b show the distribution of optimal candidate estimates considered over 2000 sample acquisitions and ten runs for the tetrahedral and hexagonal additive case studies, respectively. Observing this distribution, as opposed to the final terminal value of the optimization, provides additional insight into the regions of the candidate space that the algorithm considers as likely locations to find an optimal candidate. Since the set of real, realizable crystals is only a subset of the continuous space described by the UAFF parameters, the collection of crystals with parameter values near or within this observed distribution provides the subset of candidates that are likely to achieve a close to optimal nucleation rate. The distribution also provides a way to account for any multi-modal nature in the optimal candidate solution space.

We use the normalized UAFF parameter space described in section 2 to parameterize the candidate search space, with SW potentials for the silicon and graphene crystals used as the normalization constants for the tetrahedral and hexagonal cases, respectively. The case study for tetrahedral additives is restricted to only three out of the four UAFF parameters ($(\varepsilon_{AD}, \lambda_{SW}, \sigma_{SW})$) to maintain consistency with the ground truth data available.[37] Fromthe results, the largest peak in the optimal candidate parameter distribution is observed to be around (0.98, 1.05, 0.85) for the tetrahedral case, with a larger spread of possible candidate values in the λ_{SW} parameters. A similar spread is observed in the optimal λ_{SW} candidate estimates for the hexagonal additive case as well from Fig. 4b, thus indicating a lower sensitivity of the optimal candidate to the λ_{SW} potential. The hexagonalcandidates distribution shows a peak at (1.1, 0.41, 0.66, 1.4) with secondary peaks for ε_{SW} and ε_{AD} at $\varepsilon_{SW} = 0.36$ and $\varepsilon_{AD} = 1$.

An optimal candidate normalized parameter of near 1 indicates the suitability of silicon and graphene respectively as optimal additive candidates for the two cases. Considering this distribution of optimal candidates with peaks around (0.98, 1.05, 0.85) and (1.1, 0.41, 0.66, 1.4) thus suggests nearly optimal performance of silicon and an optimal candidate away from graphene as a nucleating agent. Both ε_{SW} and λ_{SW} are proportional to the rigidity of the crystal and smaller values (0.41, 0.66) in the case for hexagonal crystals suggests a softer and more compliant material than graphene would perform well as a nucleating agent for poly-alkanes. This result is consistent with observations from Bourque *et al.*[38] and crystal growth processes observed in semiconductors[47] where a higher compliance substrate allows for better crystal growth despite relatively large substrate-semiconductor lattice mismatch. The search for crystals with these specific deviations in SW parameters is left as a direction for future exploration.

The results from Fig. 2 and 3 highlight the non-monotonic nature of convergence of the optimization algorithm in the presence of noisy measurements. This nonmonotonicity is expected as the underlying Gaussian process model evolves in its estimate of what it thinks the optimal value will be as more data and noise realizations are made available. An initial estimate of the optimum is based on far fewer observations of the data and noise realizations. It thus can easily be misguided by noise into creating an incorrect model of the underlying ground truth, *i.e.*, suffers due to higher prediction errors. This occurrence results in a non-monotonic increase in deviation from the unknown optimum value. As further noise realizations are observed for any given candidate point, the model corrects itself and gains a better estimate for the statistics at the observed locations.

6.2 Comparison to prior-art and varying augmentation factors (p)

The noise-augmented acquisition function (32) is particularly designed to promote a higher degree of exploration in regions where fewer noise realizations have been observed to avoid getting trapped with an incorrect model of the

This journal is © The Royal Society of Chemistry and IChemE 2022

Open Access Article. Published on 07 March 2022. Downloaded on 6/18/2025 3:41:35 AM.
This article is licensed under a Creative Commons Attribution-NonCommercial 3.0 Unported Licence.

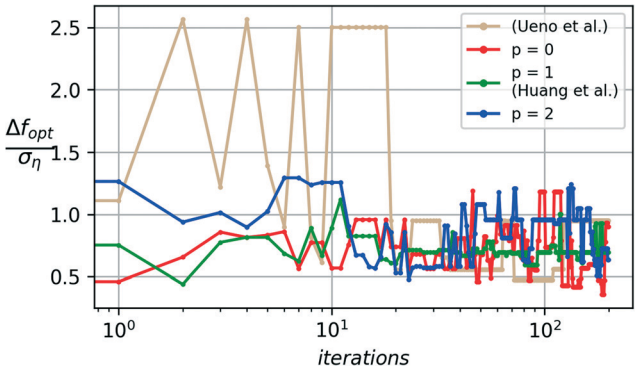

Fig. 5 A comparison of median-case performance with varying augmentation factors (p) for the acquisition function. p = 0 corresponds to the conventional expected improvement acquisition strategy for Bayesian optimization.

underlying ground truth when a noise realization misguides the algorithm. This acquisition function may result in a slower convergence as the model focuses on additional exploration to combat noise and not only on the exploitation of the model, generated from initial noise realizations, to search for optimal candidates. The augmented acquisition function, however, provides higher overall stability with improved median and worst-case performance.

Fig. 5 and 6 show a comparison of the median and worst-case performance obtained from the traditional expected improvement acquisition function (p = 0) to that of the augmented Expected Improvement function (p = 1, 2) in combating the noise-driven predictive errors from misleading of the optimization algorithm. A baseline comparison to the prior art using the toolbox from Ueno *et al.*[22] is provided.

For p = 0, a non-monotonic increase is observed in the deviation away from optimum even after 2000 iterations of the algorithm have been completed, which occurs due to the insufficient exploration of noise realizations provided by the expected improvement metric.

As the power factor p is increased in the augmented acquisition function, increased weight is provided to the exploration of noise realizations. This exploration significantly improves the worst-case performance, with fewer and smaller non-monotonic deviations upon convergence for the p = 1 case and no observable deviations upon convergence from the p = 2 case, indicating that a sufficient exploration of the noise realizations is provided by the augmented case (p = 2) before converging to an optimal candidate. This improved stability in the algorithm prevents a misleading result from being declared as optimal when the algorithm is terminated in a run where the worst-case performance might have been realized. This notion of reliability or quality of the algorithm's design choices is quantified by the quality metric Q from (20).

Fig. 7 shows the comparison for the four cases considered above in terms of the quality metric $Q(\Delta f/\sigma_\eta)$. The quality metric shows the worst-case variance in the regret obtained at any iteration in obtaining the test samples across the ten independent runs of the algorithm for each design choice. 35% of the sample budget, *i.e.*, the last 700 samples of each run are reserved as the test set to quantify the quality metric.

The quality metric shows a clear improvement in the reliability of the algorithm as the augmentation factor (p) is increased from 0 to 2. The smaller the value of Q, the smaller the variability of results obtained from the algorithm, thus higher the reliability.

6.3 Comparison across varying batch size (q)

Another important aspect in dealing with noisy and expensive material discovery experiments is that experiments are typically performed in batches. Thus the optimizer must provide a batch of candidate samples at every iteration. The Bayesian optimization algorithm is run with the noise-augmented acquisition function with p = 2 for different choices of the sampling batch size q. Ten independent runs are used to characterize the statistical performance and quality (Q) of the algorithm for each choice of q. The total number of samples drawn is kept constant at 2000 (sample budget N = 2000) to keep the results comparable. The total

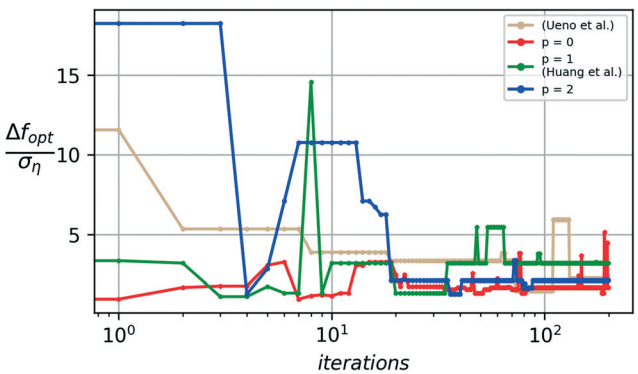

Fig. 6 A comparison of median-case performance with varying augmentation factors (p) for the acquisition function. p = 0 corresponds to the conventional expected improvement acquisition strategy for Bayesian optimization.

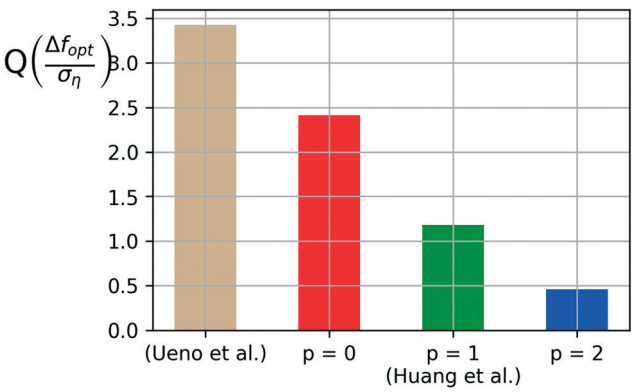

Fig. 7 Comparing model quality (Q) for varying augmentation factors (p) obtained from the test iterations with 35% of the sample budget allotted for quality testing.

Open Access Article. Published on 07 March 2022. Downloaded on 6/18/2025 3:41:35 AM.
This article is licensed under a Creative Commons Attribution-NonCommercial 3.0 Unported Licence.

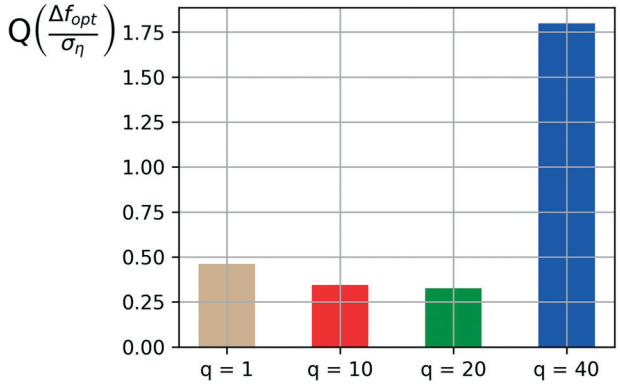

Fig. 8 Comparing model quality (Q) for varying batch sizes (q) obtained from the test iterations with 35% of the sample budget allotted for quality testing.

number of iterations available to the optimizer is then given by $2000/q$.

Fig. 8 shows a comparison of the reliability or quality metric (Q) across the different choices for the batch sizes considered. The quality metric Q is evaluated over a test set containing the last 700 samples of each independent run for a given choice of q. The figure clearly shows a marginal improvement in the algorithm's reliability as the batch size is increased from 1 to 20. A significant loss in reliability is observed as the batch size is further increased to 40.

As the batch size increases, a larger number of samples are included in the model update at every iteration, which leads to a faster accumulation of data and noise realizations on every iteration. This makes the model updates less susceptible to noise on any given iteration. The downside of larger batch sizes is that there are fewer optimizer iterations (N/q) for a fixed budget of N samples. The selection of batch size (q) is thus a tradeoff between these two factors when the total samples budget is kept constant. Fig. 8 shows this tradeoff in action with the marginal improvement of reliability up to q = 20 and a significant drop of reliability with q = 40, which leaves the algorithm with too few (50) optimizer iterations.

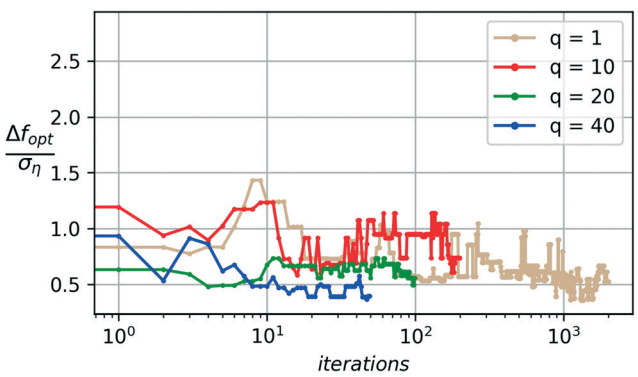

Fig. 9 Median case comparison: varying sample batch sizes (q), p = 2.

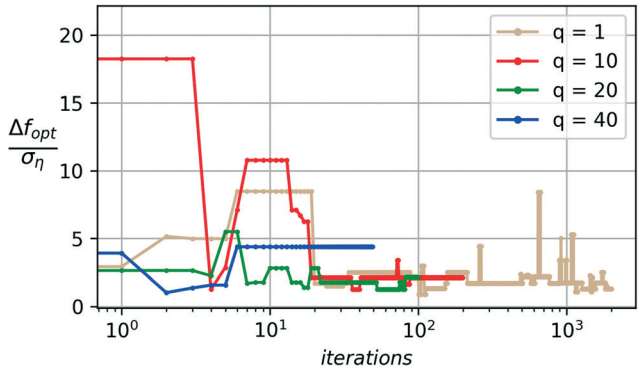

Fig. 10 Worst-case comparison: varying sample batch sizes (q), p = 2.

Fig. 9 and 10 compare the median and worst-case performances of the algorithm with varying batch size q.

The median performance (Fig. 9) sees a nearly similar error (around $0.5\sigma\eta$) across the different choices for q. The small changes in median performance upon termination are within a small fraction of the noise standard deviation and are considered statistically insignificant.

The worst-case performance (Fig. 10) however, shows consistent convergence up to q = 20 and a significant degradation of performance by several multiples of the noise standard deviation for a batch size of 40. Such a degradation occurs due to an insufficient number of optimization steps available to the algorithm for q = 40.

In practice, it is often preferred to have experiments performed in batches and thus observing consistent convergence performance with the larger batch sizes such as q = 10 and q = 20 may thus be considered optimal, as quantified by the quality metric Q and the consistent results for the median and worst-case convergence.

6.4 Observations from the numerical studies

Using the comparisons from sections 6.2 and 6.3, a batch size of q = 10 or q = 20, with p = 2, is observed to provide an adequate tradeoff with good median and worst-case performance (sub-σ and sub-3σ respectively), with an improved reliability or quality metric Q.

The numerical studies were performed using ten independent runs of the algorithm for each design choice, such as the choices for p and q. Furthermore, each independent run is initialized with an independent and randomly sampled initial training set which further contributes to the independent and randomized convergence paths taken by the algorithm across the different runs. The quality metric Q thus captures the worst-case variability of the results across all such independent runs for any given design choice of the algorithm and any sample in the last N_{test} samples acquired by a run being declared as the optimal candidate.

The Bayesian optimization with batched sampling and a noise-augmented acquisition function thus provides an effective strategy to achieve a sub-σ level of median and

This journal is © The Royal Society of Chemistry and IChemE 2022

Open Access Article. Published on 07 March 2022. Downloaded on 6/18/2025 3:41:35 AM.
This article is licensed under a Creative Commons Attribution-NonCommercial 3.0 Unported Licence.

best-case convergence in the presence of noise while maintaining a worst-case performance within three standard deviations of the noise level. The improved quality metric (Q) shows that the augmentation and batched sampling also lead to a lower sensitivity to factors such as the choice of initial training set or the choice of the termination iteration number.

7 Conclusions

This article explores the challenges in dealing with the process or measurement noise in materials discovery approaches using Bayesian optimization methods. The non-monotonic convergence and noise-driven variability of outcomes across different runs of the algorithm are shown to be significant factors to consider for the design of a Bayesian optimization approach that is robust to noise and a quality metric is introduced to quantify such variability. The use of an augmented acquisition function and a batched approach to sampling are both shown to be helpful in achieving improved robustness, and the median performance of the designed approach is shown to achieve a sub-σ level of accuracy in determining optimal candidates, while the worst-case performance shows better than 3σ level of accuracy in two case studies for additive discovery in polymer (polyethylene) nucleation.

The case studies consider the search for optimal additive candidates using a united atomic force field model for search space parameterization in classes of tetrahedral and hexagonal additives, respectively. The results suggest nearly optimal performance for silicon in the class of tetrahedral crystals but suggest a candidate more compliant than graphene in their respective classes. With the deviations observed in optimal parameters from Si and graphene, a search for possibly better-matched crystals to the discovered candidates is a direction for further research.

The augmented Bayesian optimization approach for materials discovery in noisy processes is seen to be an effective approach to minimize the number of expensive experimental or MD simulation samples required while addressing the challenges of batched sampling and robustness to noise.

Conflicts of interest

There are no conflicts to declare.

Acknowledgements

This work was supported by the National Science Foundation DMREF program under Grant No. CMMI-1729304.

Notes and references

1 J. Mockus, V. Tiesis and A. Zilinskas, in *Towards Global Optimization*, North-Holland, The Netherlands, 1978, vol. 2, pp. 117–129.
2 D. R. Jones, M. Schonlau and W. J. Welch, *J. Glob. Optim.*, 1998, **13**, 455–492.
3 M. Schonlau, W. J. Welch and D. R. Jones, in *New Developments and Applications in Experimental Design*, ed. N. Flournoy, W. F. Rosenberger and W. K. Wong, Institute of Mathematical Statistics, Hayward, California, 1998, vol. 34, of IMS Lecture Notes-Monograh Series, pp. 11–25.
4 D. D. Cox and S. John, *Proceedings of the IEEE International Conference on Systems, Man, and Cybernetics*, 1992, pp. 1241–1246.
5 J. Mockus, *J. Glob. Optim.*, 1994, **4**, 347–365.
6 M. Locatelli, *J. Glob. Optim.*, 1997, **10**, 57–76.
7 A. K. Akametalu, J. F. Fisac, J. H. Gillula, S. Kaynama, M. N. Zeilinger and C. J. Tomlin, *Proceedings of the 53rd IEEE Conference on Decision and Control*, 2014, pp. 1424–1431.
8 M. Turchetta, F. Berkenkamp and A. Krause, *Adv. Neural Inf. Process. Syst.*, 2016, pp. 4312–4320.
9 M. O. Ahmed, S. Vaswani and M. Schmidt, *Mach. Learn.*, 2020, **109**, 79–102.
10 F. Berkenkamp, A. P. Schoellig and A. Krause, *Proceedings of the IEEE International Conference on Robotics and Automation*, 2016, pp. 491–496.
11 S. S. Diwale, I. Lymperopoulos and C. N. Jones, *Proceedings of IEEE Conference on Control Applications*, 2014, pp. 1394–1399.
12 B. Letham, B. Karrer, G. Ottoni and E. Bakshy, *Bayesian Anal.*, 2019, **14**, 495–519.
13 D. Huang, T. T. Allen, W. I. Notz and N. Zeng, *J. Glob. Optim.*, 2006, **34**, 441–466.
14 P. Auer, N. Cesa-Bianchi and P. Fischer, *Mach. Learn.*, 2002, **47**, 235–256.
15 N. Srinivas, A. Krause, S. M. Kakade and M. W. Seeger, *IEEE Trans. Inf. Theory*, 2012, **58**, 3250–3265.
16 J.-Y. Audibert, S. Bubeck and R. Munos, in *Bandit View on Noisy Optimization*, Optimization for Machine Learning edn., MIT Press, 2010, ch. 1.
17 S. R. Chowdhury and A. Gopalan, in *Bayesian Optimization under Heavy-Tailed Payoffs*, Curran Associates Inc., Red Hook, NY, USA, 2019.
18 Y. Zhao, D. Zeng, A. J. Rush and M. R. Kosorok, *J. Am. Stat. Assoc.*, 2012, **107**, 1106–1118.
19 J. Snoek, H. Larochelle and R. P. Adams, *Proceedings of the 25th International Conference on Neural Information Processing Systems*, 2012, pp. 2951–2959.
20 A. Wilson, A. Fern and P. Tadepalli, *J. Mach. Learn. Res.*, 2014, **15**, 253–282.
21 E. Brochu, V. M. Cora and N. de Freitas, *A Tutorial on Bayesian Optimization of Expensive Cost Functions, with Application to Active User Modeling and Hierarchical Reinforcement Learning*, 2010.
22 T. Ueno, T. D. Rhone, Z. Hou, T. Mizoguchi and K. Tsuda, *Mater. Discov.*, 2016, **4**, 18–21.
23 P. I. Frazier and J. Wang, in *Bayesian Optimization for Materials Design*, ed. T. Lookman, F. J. Alexander and K. Rajan, Springer International Publishing, Cham, 2016, pp. 45–75.
24 Y. Zhang, D. W. Apley and W. Chen, *Sci. Rep.*, 2020, **10**, 4924.
25 A. Deshwal, C. M. Simon and J. R. Doppa, *Mol. Syst. Des. Eng.*, 2021, **6**(12), 1066–1086.

Open Access Article. Published on 07 March 2022. Downloaded on 6/18/2025 3:41:35 AM.
This article is licensed under a Creative Commons Attribution-NonCommercial 3.0 Unported Licence.

26 A. D. Bull, *J. Mach. Learn. Res.*, 2011, **12**, 2879–2904.
27 D. Pati, A. Bhattacharya and G. Cheng, *J. Mach. Learn. Res.*, 2015, **16**, 2837–2851.
28 E. Contal, V. Perchet and N. Vayatis, *International Conference on Machine Learning*, 2014, pp. 253–261.
29 H. Tran-The, S. Gupta, S. Rana and S. Venkatesh, *Proceedings of the Thirty-Fourth AAAI Conference on Artificial Intelligence*, 2020, pp. 2425–2432.
30 F. Berkenkamp, A. P. Schoellig and A. Krause, *J. Mach. Learn. Res.*, 2019, **20**, 1–24.
31 P. Larrañaga and J. Lozano, *Estimation of Distribution Algorithms: A New Tool for Evolutionary Computation*, Springer, US, New York, 2012.
32 J. Snoek, O. Rippel, K. Swersky, R. Kiros, N. Satish, N. Sundaram, M. Patwary, M. Prabhat and R. Adams, *Proceedings of the International Conference on Machine Learning*, 2015, pp. 2171–2180.
33 J. T. Springenberg, A. Klein, S. Falkner and F. Hutter, *Adv. Neural Inf. Process. Syst.*, 2016, **29**, 4134–4142.
34 J. Bergstra, R. Bardenet, Y. Bengio and B. Kégl, *Adv. Neural Inf. Process. Syst.*, 2011, **24**, 2546–2554.
35 K. Kawaguchi, L. P. Kaelbling and T. Lozano-Pérez, *Adv. Neural Inf. Process. Syst.*, 2015, **28**, 2809–2817.
36 L. Goh, K. Chen, V. Bhamidi, G. He, N. C. S. Kee, P. J. A. Kenis, C. F. Zukoski and R. D. Braatz, *Cryst. Growth Des.*, 2010, **10**, 2515–2521.
37 A. J. Bourque, C. R. Locker and G. C. Rutledge, *J. Phys. Chem. B*, 2017, **121**, 904–911.
38 A. J. Bourque and G. C. Rutledge, *Eur. Polym. J.*, 2018, **104**, 64–71.
39 F. H. Stillinger and T. A. Weber, *Phys. Rev. B: Condens. Matter Mater. Phys.*, 1985, **31**, 5262–5271.
40 W. Sun and R. D. Braatz, *Comput. Chem. Eng.*, 2020, **143**, 107103.
41 C. E. Rasmussen and C. K. I. Williams, *Gaussian Processes for Machine Learning*, MIT Press, Cambridge, Massachusetts, 2006.
42 E. Vazquez, J. Villemonteix, M. Sidorkiewicz and E. Walter, *J. Phys.: Conf. Ser.*, 2008, **135**, 012100.
43 V. Picheny, D. Ginsbourger and Y. Richet, *Proceedings of the International Conference on Engineering Optimization*, 2010, pp. 1–10.
44 N. Srinivas, A. Krause, S. Kakade and M. Seeger, *Proceedings of the 27th International Conference on Machine Learning*, 2010, pp. 1015–1022.
45 P. Frazier, W. Powell and S. Dayanik, *INFORMS J. Comput.*, 2009, **21**, 599–613.
46 S. Theodoridis, *Monte Carlo Methods*, Academic Press, London, 2nd edn, 2020, pp. 731–769.
47 F. E. Ejeckam, Y. H. Lo, S. Subramanian, H. Q. Hou and B. E. Hammons, *Appl. Phys. Lett.*, 1997, **70**, 1685–1687.

This journal is © The Royal Society of Chemistry and IChemE 2022